NOTICE

CERTAIN DATA CONTAINED IN THIS DOCUMENT MAY BE DIFFICULT TO READ IN MICROFICHE PRODUCTS.

DOE/BC/14600-13
(DE92001004)

NUMERICAL CONSTRUCTION AND FLOW SIMULATION IN NETWORKS OF FRACTURES USING FRACTALS

Topical Report

By
Yanis C. Yortsos
Jorge A. Acuna

November 1991

Performed Under Contract No. DE-FG22-90BC14600

University of Southern California
Department of Chemical Engineering
Los Angeles, California

Bartlesville Project Office
U. S. DEPARTMENT OF ENERGY
Bartlesville, Oklahoma

DISCLAIMER

DOE/BC/14600--13
DE92 001004

Distribution I

Numerical Construction and Flow Simulation in Networks of Fractures Using Fractals

Topical Report

By
Yanis C. Yortsos
Jorge A. Acuna

November 1991

Work Performed Under Contract No. FG22-90BC14600

Prepared for
U.S. Department of Energy
Assistant Secretary for Fossil Energy

Thomas B. Reid, Project Manager
Bartlesville Project Office
P. O. Box 1398
Bartlesville, OK 74005

Prepared by
University of Southern California
Department of Chemical Engineering
Los Angeles, CA 90089-1211

Contents

List of Figures

ABSTRACT

Present models for the representation of naturally fractured systems rely on the double-porosity Warren-Root model or on random arrays of fractures. However, field observation in outcrops has demonstrated the existence of multiple length scales in many naturally fractured media. The existing models fail to capture this important fractal property. In this paper, we use concepts from the theory of fragmentation and from fractal geometry for the numerical construction of networks of fractures that have fractal characteristics. The method is based mainly on the work of Barnsley [1] and allows for great flexibility in the development of patterns. Numerical techniques are developed for the simulation of unsteady single phase flow in such networks. It is found that the pressure transient response of finite fractals behaves according to the analytical predictions of Chang and Yortsos [6], provided that there exists a power law in the mass-radius relationship around the test well location. Otherwise, finite size effects become significant and interfere severely with the identification of the underlying fractal structure.

1 INTRODUCTION

Fractal geometry is a relatively new approach for the description and modeling of complex objects and processes [7], [13]. In general, fractal images are the result of the repetition of a given geometric shape into itself over a cascade of different length scales. When coupled with random noise, the resulting complexity makes fractal images suitable for the description of a variety of natural objects. Although this should not imply that every such object is fractal, nonetheless fractals constitute a very convenient method to describe many physical processes. In particular, the application of fractals to porous media is very promising. The review by Sahimi and Yortsos [17] classifies the fractal patterns that result from various porous media processes, such as percolation, viscous fingering and fracturing. Networks of fractures in a rock are natural candidates for a fractal geometry description. This particular alternative is explored in this paper.

Conventionally, naturally fractured systems have been represented by the Warren and Root double porosity model [21] or by a random array of fractures [5], [12]. Although capturing important properties, neither of the two geometries can account for fractal characteristics recently attributed to naturally fractured systems [2], [16], [18]. The relation of fractals to fracture net-

works was first explored in 1985, in a study of nuclear waste disposal [2]. That study revealed that many fracture patterns at Yucca Mountain, NV, were self-repetitive over a range of scales, spanning from 0.2 to 15 meters, within which several generations of fractures were detected. Additional support for the fractal character of fracture networks can be found in recent studies of the fracture patterns of the Monterey formation [8] and of the Geysers geothermal field [19]. Prominent fractal features in the latter include the existence of a cascade of fracture scales and a self-similar structure.

It was recently proposed that the fracturing of disordered media, such as natural rocks, can be modeled using fractals [10], [20]. Indeed, fractal structures have been related to the fracture resistance of the material and to the particular fracturing process it undergoes [20]. For example, fragmentation with substantial shearing, which appears to be a dominant mechanism for many fracture networks, leads to fractal dimension values ranging between 1.2 and 1.8, [4]. Sammis et al. have reported fractal dimensions between 1.5 and 1.7, [18].

Motivated by such findings, investigators have recently attributed fractal properties to networks of fractures and proceeded to analyze their hydraulic response (Chang and Yortsos [6], Beier [3]). These works demonstrated that the traditional solutions for single-phase fluid flow are particular cases of a more general solution, where the dimensionality (reflected in the fractal dimension) is a key variable. Significantly, this dimension can take non-integer values and characterizes the fractal response.

Current studies in the modeling of fractured systems with fractals rely on Sierpinski carpets and percolation networks [15]. In certain cases, numerical simulation has shown the expected for a fractal transient response. However, the particular networks taken represent rather special and idealized cases. Fractal models for naturally fractured systems must be consistent with the basic mechanisms of fracturing, such as shear fracturing, extension fracturing, etc. [11]. In addition, any synthetic network must honor available data, such as fracture length distribution, fracture orientation and density, etc. Real systems also possess upper and lower cutoffs, which place limits on the range of fractal behavior. Strictly speaking, rigorous methods for the construction of networks of fractures must await the successful development of fracturing theories. Recent advances in this area have been many and significant and they hold promise that a unified theory may soon emerge [10].

A practical alternative that may lack in rigor, but affords great flexibility, is possible for

systems that may be described by a fragmentation process. The latter is known to lead to fractal size distributions [20]. The essential aspects of fragmentation can be simulated with the application of the IFS (Iterated Function System) approach introduced by Barnsley [1]. This technique yields networks of the desired fractal properties with much flexibility in the orientation of the fractures and in the shapes of the fragments. This approach of combining fragmentation and IFS to create fractal networks is proposed in this paper. Two issues will be addressed:

(i) The numerical construction of a synthetic network of fractures with fractal characteristics.

(ii) The simulation of transient, single-phase flow of a slightly compressible fluid and its pressure transient response in such networks.

2 NUMERICAL SYNTHESIS OF FRACTAL NETWORKS OF FRACTURES

2.1 FRAGMENTATION AND FRACTALS

In many fragmentation processes, the distribution of fragment sizes can be described by a power law. This fact has been known since the early 1940s, when Schuhmann's law [9] was introduced to describe the distribution in grinding operations. Turcotte [20] documents many fracturing applications, where the size distribution is described by a power law. More recently, Poulton et al. [16] postulated a power law behavior not only for the fragment size, but also for the length and spacing of discontinuities in the rock. In a related study, a power law distribution of fracture trace lengths was discovered by Barton [2].

Fragmentation was modeled in the classical work of Gilvarry [9], who used an exponential distribution to describe repetitive fracturing. A basic parameter in the analysis is the probability $p_f(l)\delta l$ that a given fragment of size in the interval between l and $l+\delta l$ will be fragmented. Recently, Turcotte [20] has showed that when p_f is constant, a power law distribution of fragment sizes is obtained. For an idealized fragmentation process, where the fragments of a given generation are all of the same relative size, the fragment size distribution is of the power law type, with an exponent related to the probability of fracturing p_f. For example, if each block creates an average of Sp_f new blocks of relative size $1/S$, the theoretical value of the exponent is

$$E = \frac{2 \ln S p_f}{\ln S} \tag{1}$$

It can be shown that this exponent is also equal to the box fractal dimension, D, of the mosaic made up of the same pieces. Since an unfractured block represents a missing subset of fractures, the fracture length distribution will also be power law distributed with the same exponent. Equation (1) suggests that non-trivial fractals ($D < 2$) are obtained only for $p_f < 1$.

The box counting fractal dimension is one measure of a fractal structure. It is typically calculated by superposing a grid of a given cell-size on the fracture pattern and by counting the number of occupied cells. The power law relation

$$N(r) \sim r^{-D} \tag{2}$$

between the number $N(r)$ of occupied cells and the scale r, yields the dimension D. Box counting has been routinely used to characterize the fractal properties of real networks [2], [18].

For more realistic fragmentation processes, blocks of a given generation are not all of the same relative size and a given size group may be composed by blocks of different generations. Nonetheless, as will be shown later, a power law distribution in fragment size and fracture length still persists. We should also add that fractal behavior typically holds in a finite range between an upper and a lower cutoff scale. The upper cutoff is defined by the maximum size fragment (the "largest hole" in the network). The lower cutoff is more arbitrary, usually decided from practical considerations. As shown below, finite cutoffs play an important role in the hydraulic response.

The way by which patterns are created by fragmentation, namely the initiation from a large scale and the propagation towards successively smaller scales in a systematic manner, has a close analogy with the IFS technique recently developed. In the following, we propose to mimic a natural fracturing process in the construction of a synthetic network by combining the IFS with a probability rule.

2.2 GENERATION OF FRACTAL NETWORKS OF FRACTURES

Barnsley [1] has recently proposed the method of Iterated Function System (IFS) to construct fractal images. With this technique, a fractal is obtained from an initial simple shape (initiator)

by applying in an iterative fashion a set of numerical transformations (propagator). Each iteration creates multiple sets of n smaller, transformed images that occupy the place of the previous image. After several generations the set converges to a fractal. The technique creates fragments of various sizes and shapes and it is well suited for the development of synthetic networks of fractures.

For the creation of the two-dimensional patterns to follow, two transformations were used. Each consists of two quadratic expressions

$$x_n = ax_{n-1} + by_{n-1} + cx_{n-1}y_{n-1} + d$$

$$y_n = ex_{n-1} + fy_{n-1} + gx_{n-1}y_{n-1} + h$$

where x_n, y_n are the coordinates of a given point of the nth generation, and a,b,c,d,e,f,g,h are the coefficients of the transformation. When $c = g = 0$ the transformation is linear (generally self-affine). If in addition $a = f$ and $b = -e$, it gives rise to self-similar fractals. The non-linear terms (c, g) are useful in controlling the geometry of the final pattern. However, control of the fractal characteristics and the fractal dimension is mainly obtained by varying the probability p_f. As in fragmentation, we may specify that a fraction $1 - p_f$ of newly generated blocks is not allowed to further subdivide. The value of p_f affects the fractal dimension, although not necessarily according to the simple result in equation (1).

Figures 1, 2 and 3 show three typical examples of fracture networks obtained with the application of self-similar, self-affine and non-linear transformations, respectively. A fracturing probability $p_f = 0.75$ was applied every second generation. Because of our interest on fracture networks, the objects of Figure 1 to 3 have their fractures retained. Thus, they are not strictly self-similar or self-affine. In this regard, they represent modifications of the well-known Sierpinski gasket [13]. Nevertheless, they do possess similar fractal characteristics. Figures 1b, 2b and 3b show plots of the box counting, fracture length and fragment size distributions corresponding to these objects. In all objects, box counting exhibits a power law behavior reflecting the underlying fractal structure, with an exponent varying between the values of 1.60 (for Figure 1b) and 1.62 (for Figure 3b), both very close to the theoretical value of 1.59 for a Sierpinski gasket. For the object of the self-similar transformations of Figure 1a, the other two fractal measures (fracture length and fragment size) are step-like with steps of equal size. If only the points at the edges of the step are taken, the discrete distribution so obtained is of the power

law type with an exponent consistent with the theoretical value. However, this is not the case for Figure 2b, where fracture length and box counting give approximately the same exponent but the fragment size distribution hardly resembles a power law. It must be noted that finite size effects are present on all distributions. The third non-linear object of Figure 3a can be characterized as fractal, if box counting is applied ($D \sim 1.62$). Fracture length still follows a fairly well defined power law. However, fragment size distribution has a power law behavior only in segments. Certainly, as more generation are included, the distributions approach the expected power law. The above differences serve to emphasize the relevance of box counting in the characterization of the fractal structure in finite fractals.

The shape and geometry of the initiator have a significant effect on the geometry of the final pattern. Figure 4a shows a pattern of eleven generations initiated from a quadrilateral shape with a single fracture. Physically, the transformation at each stage consists of a rotation and subdivision of the original two (upper or lower, left or right) halves. The apparent relative complexity of this pattern hides the fact that there are only minor differences with Figures 1 to 3, namely the angle of the initial fracture, the initial shape and the value of p_f (here equal to 1). In Figure 4a the initial fracture tends to be parallel to the top and bottom edges. Corresponding box counting, fracture length and fragment size distributions are shown in Figure 4b. Because the pattern is composed of pieces in a narrow size range, the box counting fractal dimension is very close to 2 in the range of interest. Changing the position of the initial fracture dramatically alters the final pattern. Figure 5a corresponds to the same initiator shape as Figure 4a, except that the initial fracture is tilted at a larger angle. In this highly distorted network, the initial fracture is hardly recognizable.

Even though Figures 4 and 5 appear realistic, as more generations are included, the fracturing process continues until the medium completely disintegrates. This results from the fact that each block was allowed to further subdivide ($p_f = 1$). To obtain non-trivial fractal patterns, the fragmentation probability must decrease, lower values in p_f resulting into lower values of the box counting dimension D. The patterns in Figures 6a and 7a were constructed as in Figure 4a, except that a fraction $(1 - p_f)$ of randomly selected fragments were left unfractured after the fourth generation. Different selections of the fragments result into different networks, although all realizations have the same box counting fractal dimension. Figure 6b and 7b show the box counting, fracture length and fragment size distributions for these patterns. The box dimen-

sions are 1.78 and 1.65 for the two networks, respectively. As expected, the values depend on both p_f and the particular geometry. Away from the cutoffs, fragment size and fracture length distributions are of the power law type. Finite size effects are limited to sizes close to the cutoffs for regular and moderately distorted networks.

The sequence of transformations that creates a fracture also specifies its address. For example, if an IFS of two transformations, denoted by 0 and 1 respectively, is used, typical addresses of fractures are 001, 1010, 01101, etc. The number of digits in the sequence equals that of the generation to which the fracture belongs. The numbers also determine the position of a particular fracture in the map. This systematic fracture identification is especially appropriate for fluid flow simulation. The networks presented in this paper were constructed with two transformations applied to a two-dimensional initiator consisting of a single initial fracture in a quadrilateral shape. Of course, this is not a limitation of the technique, which allows for an infinite variety of transformations in any dimensions and for any initiator.

3 FLUID FLOW SIMULATION

The usefulness of any synthetic network is tied to the ability to simulate fluid flow. In the networks under consideration, the IFS technique allows for expedient simulation. Certainly, for a numerical solution, a finite number of generations must be considered. As shown below, this imposes a significant constraint.

3.1 FLOW CONDUCTIVITY MATRIX

The unique binary sequence that identifies each fracture, makes possible to precisely specify its address, shape and location, as well as to devise a numbering system for its end points. In this fashion, the nodes of the network are directly identified. This is an important development, as it alleviates the need for a finite-difference or a finite-element description. Moreover, it is uniquely related to the self-similar, nested structure of the fractal object.

To proceed with flow simulation, certain assumptions regarding the fluid flow in the fractures must be made. Consider single phase flow. Along each fracture, the usual expression applies:

$$Q = C\rho W^{\lambda}[\frac{\Delta p}{l}] \tag{3}$$

where Q is the mass flow rate, W is the width of the fracture, Δp is the pressure drop along the fracture, ρ is the fluid density and λ is the conductivity exponent, usually taken equal to three. To construct the flow conductivity matrix, we make use of the address of each fracture. The two end nodes of the initial fracture, of known coordinates, are numbered nodes 1 and 2. Each new fracture subdivides an existing block and adds two new nodes to the system. The general expression for the number of the end nodes of a fracture are α and $\alpha + 1$, respectively, where

$$\alpha = 2^{j+1} - 1 + 2 * (ad) \tag{4}$$

Here, j is the generation to which the given fracture belongs, and ad is the decimal value of the binary address. The coordinates of each such node are obtained by applying the sequence of transformations described by the address to the coordinates of nodes 1 and 2. In this fashion, we may obtain the coordinates and the number of each node in the network. Intersections between fractures are also specified numerically in a simple manner. The final step is to calculate the conductivity of each fracture according to the assumptions made and to fill the entries of the conductivity matrix.

A true fractal pattern of fractures contains an infinite number of generations. In practice, however, only a small number of generations can be considered, since the size of the conductivity matrix doubles with every additional generation. This limitation is very significant on the response of the fractal.

3.2 PRESSURE TRANSIENTS

We subsequently considered the simulation of the pressure transients during drawdown. A single well is assumed, producing at constant rate, with no flux boundary conditions imposed at the sides of the pattern. Flow occurs only in the fractures. The flow between nodes was evaluated using (3), while an appropriately weighted volume was assigned to each node. For simplicity, each fracture was assigned the same width. Denoting by g_{ij} the conductance between neighboring nodes i and j, the following discrete form for the mass balance for node i can be readily derived

$$c_f \rho_i V_i \frac{\Delta p_i}{\Delta t} = \sum_j \frac{\rho_i g_{ij} (p_j - p_i)}{\mu (_{ij}} - Q \delta_{i,m} \tag{5}$$

where subscript j denotes all nodes connected to node i, c_f is the fluid compressibility and m is the node number of the well. We have also used the shorthand notation $\delta_{i,j} = 1$ for $i = j$ and $\delta_{i,j} = 0$ for $i \neq j$. For further simplicity, we take the approximation $V_i = \frac{1}{2}\sum_j A\ell_{ij}$, and $g_{ij} = Ak$, where k is the fracture permeability. Defining dimensionless variables $p_D = \frac{2\pi(p_{in}-p)\rho_0 kA}{Q\ell\mu}$, $\ell_{D,i,j} = \frac{\ell_{ij}}{\ell}$ and $t_D = \frac{kt}{\ell^2 c_f \mu}$, where ℓ is the average size of fractures of the last generation and $\rho_D = \frac{\rho}{\rho_0}$, where ρ_0 is a reference density, we finally obtain

$$\frac{\rho_{D,i}}{2\Delta t_D}\sum_j \ell_{D,ij}\Delta p_{D,i} = \sum_j \rho_{D,ij}\left(\frac{p_{D,i}-p_{D,j}}{\ell_{D,ij}}\right) + \delta_{i,m} \tag{6}$$

This set of equations was solved using a fully implicit algorithm which iterates on the density term at each time step.

Of crucial importance to the solution of the above is the size ratio $N = \frac{L}{\ell}$, where L is the physical size of the domain. N is also related to the total number of nodes (approximately proportional to $\frac{2}{Z}N$, where Z is the coordination number of the network). A theoretical fractal corresponds to $N \gg 1$ (obtained for infinitely many generations). However, as pointed out above, practical considerations restrict N to a smaller value ($O(100)$).

It is important to discuss the effect of ℓ. When the number of generations of fractures in the network increases for a fixed L, this is equivalent to a decrease in ℓ, and to an increase in N. In the dimensionless notation above, the effect will be equivalent to an increase in the size of the system, or to a delay of the boundary effect. It follows that, working with a large a number of generations is beneficial in two ways: It not only assigns stronger fractal characteristics to the network, it also serves to delay the effect of the boundary on the pressure transient. On the other hand, by decreasing ℓ, the real pressure and real time corresponding to fixed dimensionless values also decrease, the real time following an ℓ^2 dependence. It is possible that this may render more difficult the actual identification of the fractal structure, because of the demand for an increased resolution of the diagnostic instruments, particularly when the fracture permeability is high.

The solution of (5) can be expressed solely in terms of N and t_D

$$p_{D,m} = f(t_D; N) \tag{7}$$

Theoretically ($N \gg 1$), a fractal system must respond as described by the power law of Chang and Yortsos [6]

$$p_{D,m} \sim t_D^{\frac{1}{2}-\lambda} \tag{8}$$

where $\delta = \frac{d_s}{2}$ and d_s is the spectral dimension. For percolation networks, d_s is related to the mass fractal dimension D and the fractal dimension of the random walk d_w [17] through

$$d_s = \frac{2D}{d_w} \tag{9}$$

Equivalently, we may use $\theta = d_w - 2$ to write

$$\delta = \frac{D}{2+\theta} \tag{10}$$

While D is an expression of the mass dimension, θ is related to the network connectivity and describes the deviation from an ordinary random walk in the fractal network. Clearly, it is the combination of both these parameters that contributes to the fractal response.

Contrary to the theoretical results, however, the numerical simulation is subject to finite size effects. These are particularly notable when the well is "off-centered" as explained below. To analyze such effects, we focused our sensitivity studies on the number of generations, the position of the well and the randomness and irregularity of the pattern. As a diagnostic of true fractal behavior we used the pressure response in a log-log plot. According to the theory, the plots of log p_D and $dp_D/d\log t_D$ vs log t_D must both be linear. Equivalently, we may monitor the slope of these curves and test whether they are constant or not.

For a Euclidean homogeneous network, both slopes should approach zero after an early transient. This is indeed the case as shown in Figure 8. The early response with slope of $\frac{1}{2}$ is present in all our simulations, indicating flow in a single (or a few) fractures that directly feed the well. It is interesting to note that it is often the second curve (second derivative) that allows a clearer identification of the underlying structure (it approaches a constant value faster). Also shown in Figure 8c is the radial total fracture mass plot corresponding to this regular network. The plot is obtained by tracing circles of increasing radius around the well and by measuring the cumulative fracture length within each such circle. In the homogeneous case we expect a radial slope of 1 at small radii (single fractures originating from the well site) and a slope of 2 at larger values, characteristic of homogeneous systems. This is indeed displayed in Figure 8c.

For a fractal network, the theoretical fractal behavior is well displayed in Figure 9, which shows the transient response of a well at the center of the modified Sierpinski gasket of Figure 1. After an early transient, the two slopes remain constant for a significant interval of time, until boundary effects are felt (Figure 9b). The constant slope is a clear indication of an underlying

fractal structure. In fact, the slope approaches the theoretical value of 0.26 ($\delta = 0.74$), for $D = 1.59$ and $\theta = 0.16$. This value of θ was obtained by random walks on the network as described by Orbach [14]. The numerical values of δ and θ are also in agreement with fluid flow simulations performed in modified Sierpinski carpets [15].

The fractal response is a consequence of the well developed radial fractal structure around the well under consideration. We confirm this in the associated radial mass plot (Figure 9c) which shows two segments, one for small radii with slope 1, related to the early transient, and another at larger radii with slope 1.59, related to the later part of the transient response. For finite size systems, radial fractal structure is necessary in order to counteract finite size effects.

The modified Sierpinski gasket was next taken to investigate the effect of the number of generations. The transient response for a gasket with nine (two less) generations is shown in Figure 10a. The early behavior in both Figures 9 and 10 is identical. However, because of the additional length scale, the response of Figure 9 is extended over a longer period of dimensionless time (one more cycle), thus making easier the identification of the constant slope period. This result is consistent with the previous analysis.

Finite size effects can be introduced by slight rearrangements, for instance by placing the test well at an "off-centered" position. Figure 11 shows the transient response for a test well placed at position B in the object of Figure 1a. It is observed that the early transient of $\frac{1}{2}$ slope is prolonged, while the period of constant fractal slope appears later and it has much shorter duration. The slope value is also slightly lower than in the case of position A. An explanation of this behavior is as follows. For finite systems, the development of a sharp response depends on how well a power law fits the radial mass relationship around the test well. For a perfect fractal, this relationship is of the power law type with an exponent equal to the mass dimension D ($D < 2$). This is not the case for our finite networks. For location B, the radial mass plot shows at least three segments. The first with slope of 1 is longer than the corresponding segment for position A. This accounts for the longer lasting period of the early transient at position B. The last two segments of the radial mass plot, with slopes 2.24 and 1.72 respectively, can be related to respective features in the derivative slope curve (dashed curve). However, if the network of Figure 1a were a subset of a larger self-similar network, a power law radial mass plot and a fractal transient response would still have been observed, much like in a true fractal, regardless of the position of the well.

In general, the response of finite systems vary significantly with the arrangement of the matrix blocks (computationally obtained by taking different realizations). It appears that if the blocks are arranged so that the radial structure around the well possesses fractal characteristics, the response is also fractal. This is consistent with the theoretical results, which assume radially fractal characteristics [6], and with the findings of [15].

Pressure transient tests were also conducted for the networks of Figures 6 and 7. The square dot in the middle of the pattern indicates the position of the test well. Results are shown in Figures 12 and 13, respectively. Although both pressure responses are very different from the homogeneous case (compare with Figure 8), neither test conforms exactly to the theoretical expectations for a fractal. The well of Figure 6 has a response that tends to a constant slope, this behavior being consistent with the radial mass plot which has certain power law segments. However, it cannot be used to unambiguously ascertain the underlying fractal. Even less revealing is the response of the well of Figure 7, where the approach to a constant value occurs late and it is interfered with boundary effects. It should be stressed again that this departure from the theoretical expectations is only a result of the limited number of generations allowed in the numerical computations (the objects of Figures 6 and 7 have fractal characteristics over a small range of scales only). Coupled with the irregularity and randomness of the patterns, this limitation prevents the identification of the fractal structure. On the other hand, many real systems are more likely than not to contain such limitations. Further work is necessary to develop better diagnostic techniques for the identification of such networks.

A variety of other tests were also performed and analyzed. The previous findings were consistently confirmed, namely that as long as the number of generations is small, the transient response is unlikely to have the theoretical characteristics, unless the arrangement of matrix blocks is such that a radially fractal structure exits.

4 CONCLUSIONS

A method to create fractal fracture networks with fractal characteristics was developed. The method is based on a combination of the IFS technique for constructing fractal images [1], and of a probability rule consistent with a fragmentation process. This technique allows one to create two-dimensional fractal networks with controlled fragment shape, upper and lower

cutoffs, fragment sizes, and fractal dimension. Although not attempted here, the method can be generalized for the creation of three-dimensional networks.

The simulation of pressure transients showed that the identification of the fractal object with the help of existing theoretical methods is possible only if a significant number of generations is allowed, or, equivalently, if the object is fractal over a large enough range of scales. Otherwise, finite size effects and randomness may dominate the pressure response and make difficult the identification of the structure. This behavior serves to emphasize the importance of cutoff scales in fractals.

NOMENCLATURE

ad = decimal value of binary number

A = area of fracture, L^2

c_f = fluid compressibility, $LM^{-1}T^2$

D = box counting fractal dimension

g_{ij} = conductivity of fracture that joints nodes i and j,L^4

k = permeability of fracture, L^2

L = size of medium, L

ℓ = average size of fractures of last generation, L

ℓ_D = dimensionless length

p = pressure, $L^{-1}MT^{-2}$

p_{in} = initial pressure, $L^{-1}MT^{-2}$

p_D = dimensionless pressure

p_f = probability of fracturing for fragment of given size

Q = mass flow rate, MT^{-1}

r = size, L

S = fracturing parameter

t_D = dimensionless time

V_i = fracture volume associated to node i, L^3

W = fracture width, L

α = node number

δ = parameter in fractal fluid flow formulation

$\delta_{i,j}$ = source term for dimensionless notation

Δp = pressure drop, $L^{-1}MT^{-2}$

Δt_D = dimensionless time increment

λ = conductivity exponent for fractures

ρ = density of fluid, ML^{-3}

θ = conductivity index

μ = viscosity, $L^{-1}T^{-1}M$

ACKNOWLEDGMENTS

This research was also supported in part by the Center for the Study of Fractured Reservoirs supported by the California State Land Commission, Oryx, Shell, E & P, Texaco and Unocal. We thank Professor I. Ershaghi for useful discussions. Computer time for the numerical simulations was donated by the NSF San Diego Supercomputer Center.

References

[1] M.F. Barnsley. *Fractals Everywhere*. Academic Press, Boston, 1988.

[2] C.C. Barton and P.A. Hsieh. Physical and hydrologic-flow properties of fractures. field trip guidebook t385. In *28th International Geological Congress*. American Geophysical Union, 1989.

[3] R.A. Beier. Pressure transient field data showing fractal reservoir structure. *SPE Paper 20582 presented at the 65th Annual SPE Fall Meeting, New Orleans, LA, Sept. 23-26*, 1990.

[4] W.K. Brown, R.R. Karpp, and D.E. Grady. Fragmentation of the universe. *Astrophysics and Space Science*, 94, 1983.

[5] M.C. Cacas, E. Ledoux, G. deMarsily, and B. Tillie. Modeling fracture flow with a stochastic discrete fracture network: Calibration and validation. 1 the flow model. *Water Resources Research*, 26:479–489, 1990.

[6] J. Chang and Y.C. Yortsos. Pressure-transient analysis of fractal reservoirs. *SPE Formation Evaluation*, page 631, 1990.

[7] J. Feder. *Fractals*. Plenum Press, New York, 1988.

[8] R.E. Garrison, editor. *The Monterey Formation and Related Silicieous Rocks of California*. The Pacific Section Society of Economic Paleontologists and Mineralogists, Los Angeles, 1981.

[9] J.J. Gilvarry. Distribution of fragment size in repetitive fracture of brittle solids. *Solid State Communications*, 2:9, 1964.

[10] H.J. Herrmann and S. Roux. *Statistical Models for the Fracture of Disordered Media*. North Holland, 1990.

[11] J.C. Jaeger and N.G.W. Cook. *Fundamentals of Rock Mechanics*. Chapman and Hall, London, 1979.

[12] J.C.S. Long and K. Hestir. An analytical expression for the permeability of random two-dimensional poisson fracture networks. *Lawrence Berkeley Laboratory Earth Sciences Division Annual Report 1989*, pages 45–48, 1990.

[13] B.B. Mandelbrot. *The Fractal Geometry of Nature*. W.H. Freeman, New York, 1983.

[14] R. Orbach. Dynamics of fractal networks. *Science*, 231:814–819, 1986.

[15] J. Polek, K. Karasaki, J.C.S. Long, and J. Barker. Flow to wells in fractured rock with fractal structure. *Earth Sciences Division Annual Report 1989 Lawrence Berkeley Laboratory*, 1990.

[16] M.M. Poulton, N. Mojtabai, and I.W. Farmer. Technical note: Scale invariant behavior of massive and fragmented rock. *Intl.J. Rock Mech. Min.Sci. and Geomech.*, 27:219, 1990.

[17] M. Sahimi and Y.C. Yortsos. Application of fractal geometry to porous media: A review. *Paper SPE 20476 presented at the 65th Annual SPE Fall Meeting, New Orleans, LA, Sept. 23-26*, 1990.

[18] C. Sammis, G. King, and R. Biegel. The kinetics of gouge deformation. *PAGEOPH*, 125:777, 1987.

[19] C. Sammis, J. Lin, and I. Erhsaghi. Feasibility of fractal characterization of The Geysers geothermal field. *Proceedings of the 16th Workshop on Geothermal Reservoir Engineering Stanford, CA, Jan. 23-25*, 1991.

[20] D.L. Turcotte. Fractals and fragmentation. *Journal of Geophysical Research*, 91(B2):1921, 1986.

[21] J.E. Warren and P.P. Root. The behavior of naturally fractured reservoirs. *SPEJ*, page 245, 1963.

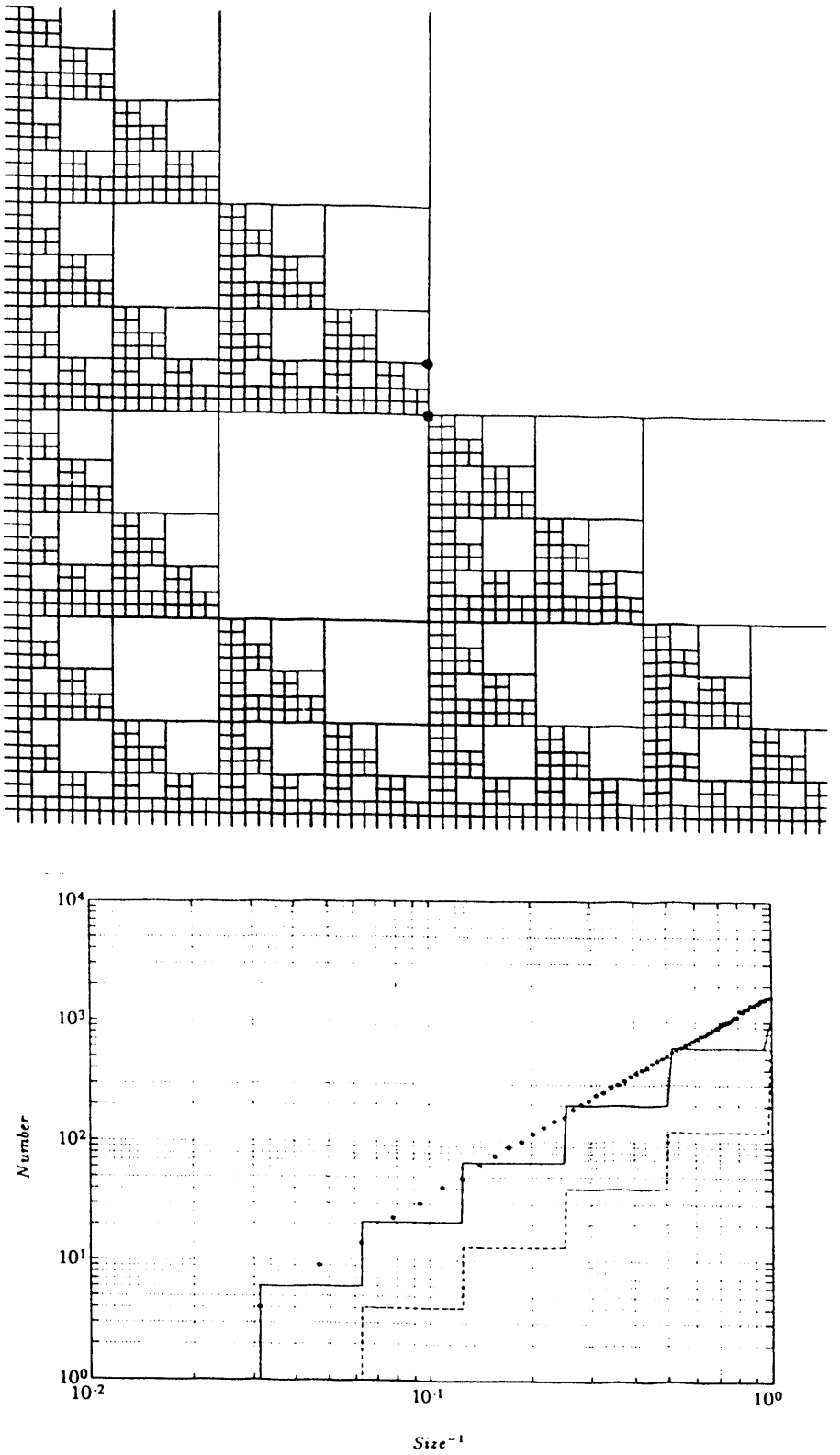

Figure 1: (a) Modified Sierpinski gasket (11 generations) with self-similar IFS. Positions A (square) and B (circle) (b) Corresponding box counting(*), fracture length (solid line) and fragment size (dashed line) distributions.

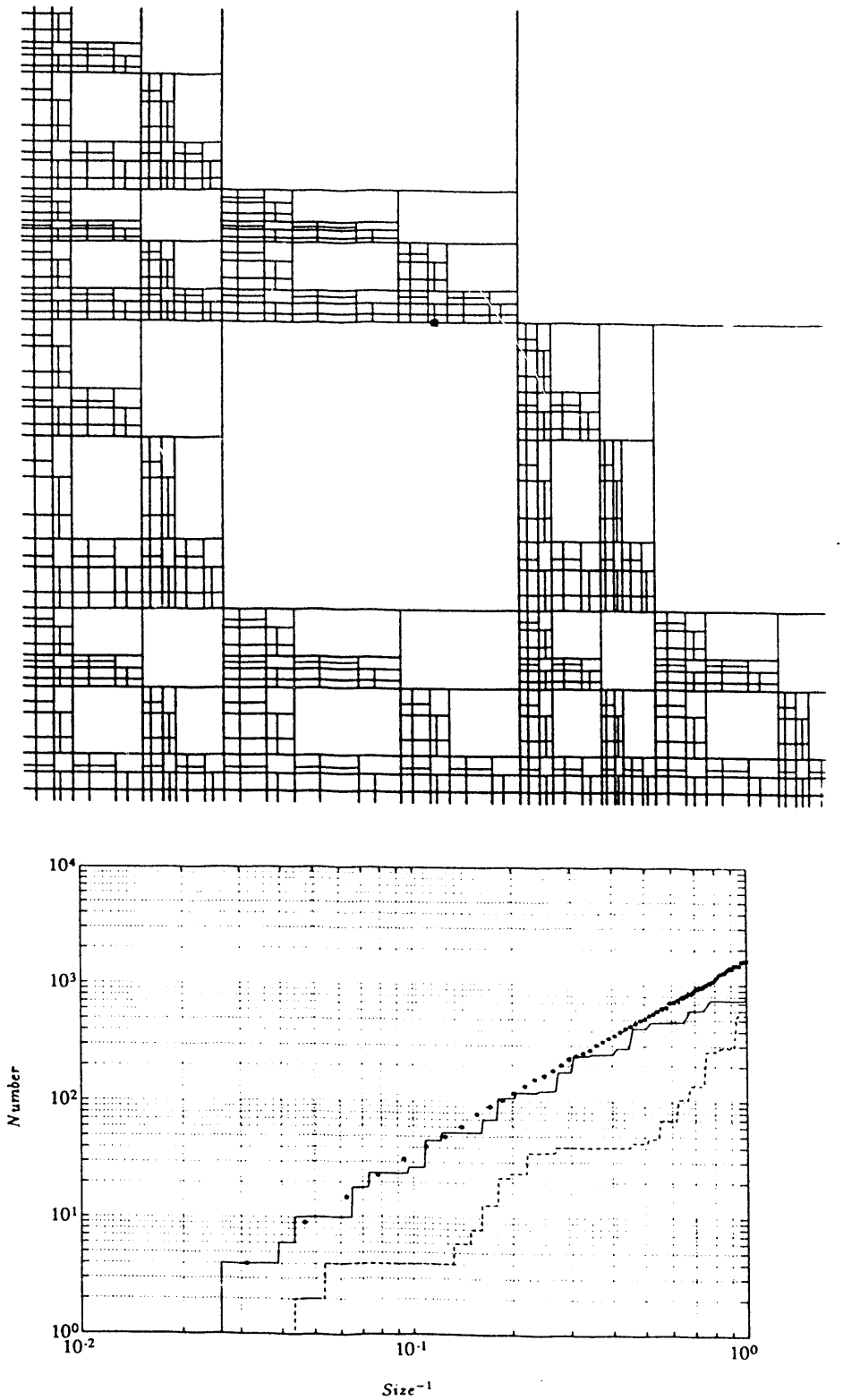

Figure 2: (a) Modified Sierpinski gasket (11 generations) with self-affine IFS. (b) Corresponding box counting(∗), fracture length (solid line) and fragment size (dashed line) distributions.

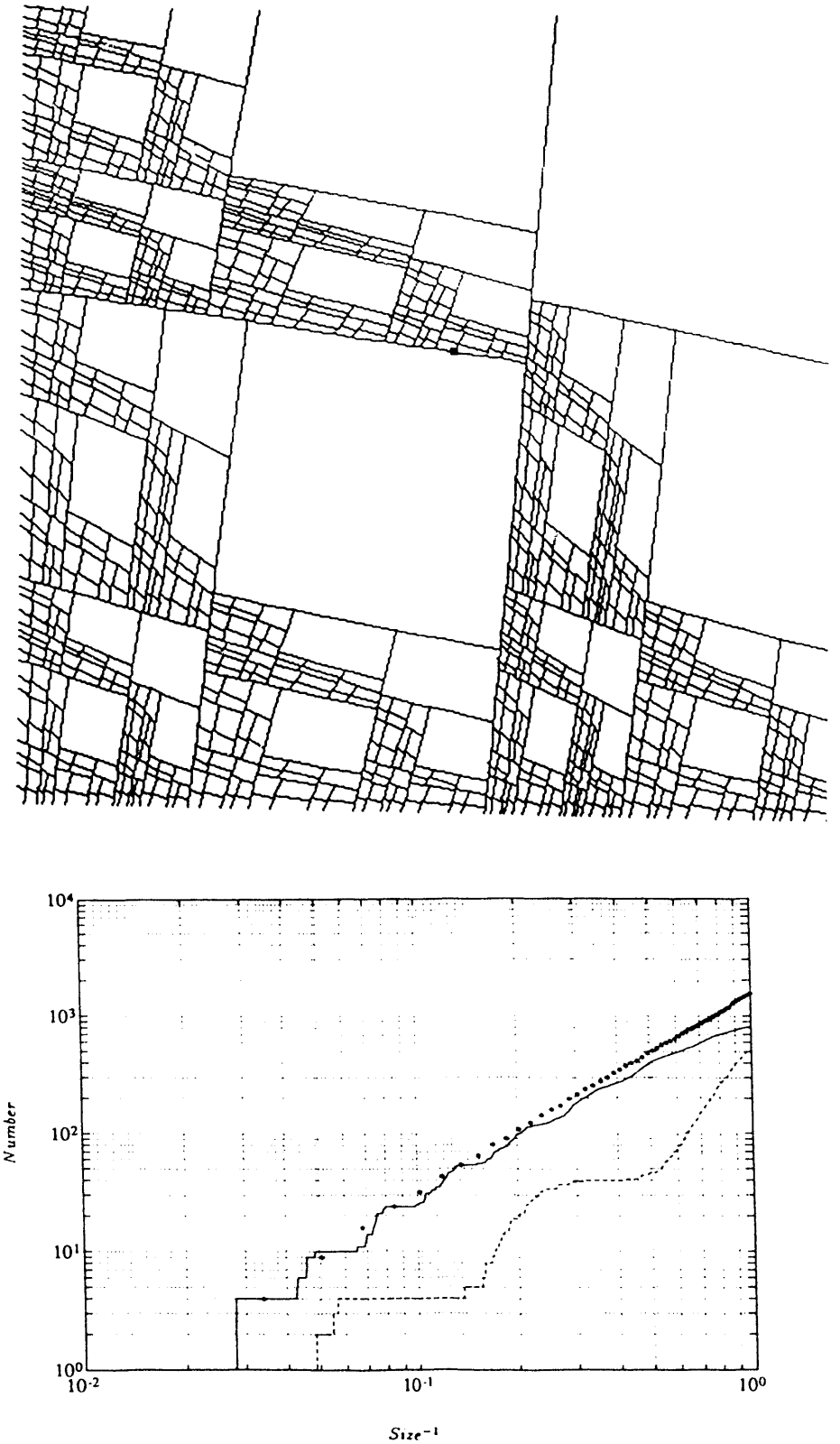

Figure 3: (a) Modified Sierpinski gasket (11 generations) with non-linear IFS. (b) Corresponding box counting(*), fracture length (solid line) and fragment size (dashed line) distributions.

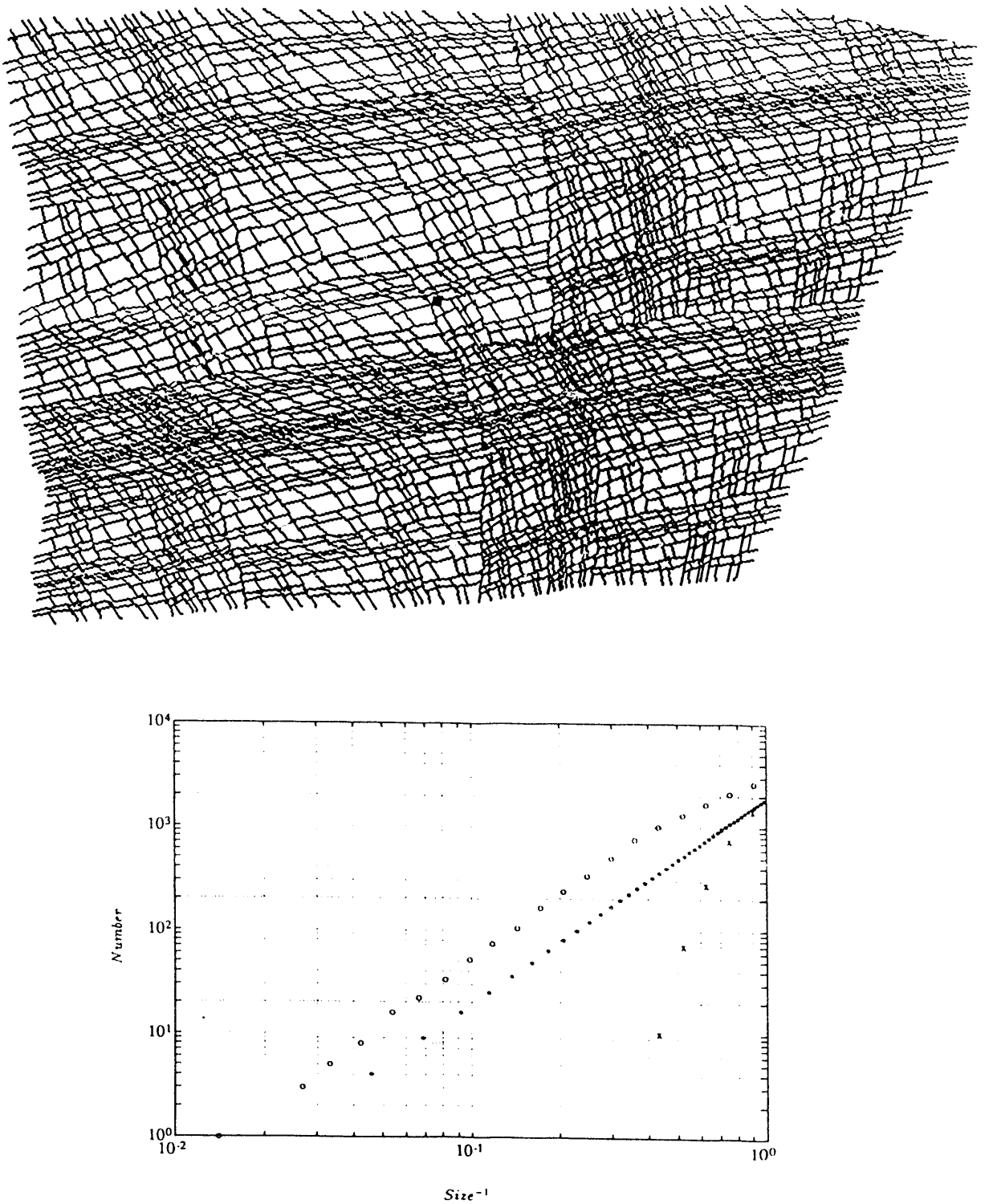

Figure 4: (a) Fracture network (11 generations) using a quadrilateral initiator and $p_f = 1$. (b) Corresponding box counting($*$), fracture length(o) and fragment size (x) distributions.

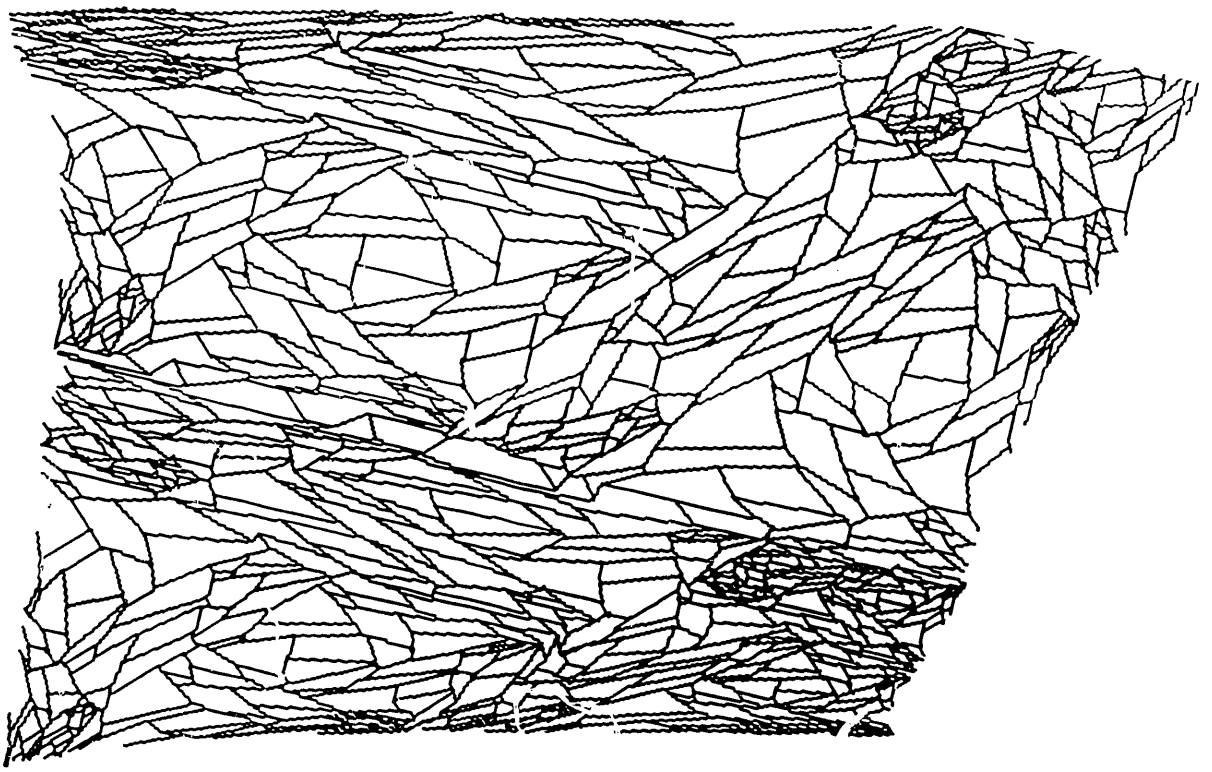

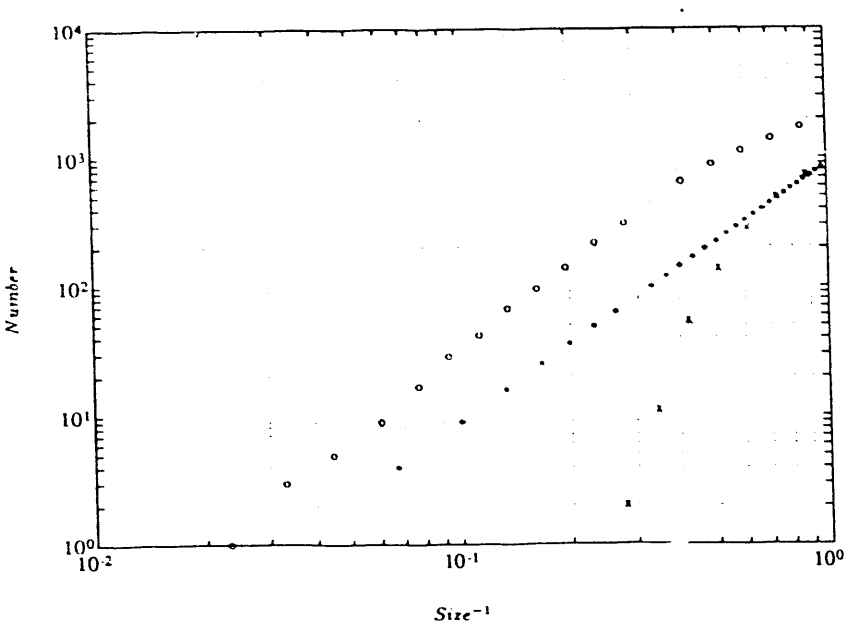

Figure 5: (a) Distorted fracture network (11 generations) using a quadrilateral initiator and $p_f = 1$. (b) Corresponding box counting ($*$), fracture length(o) and fragment size (x) distributions.

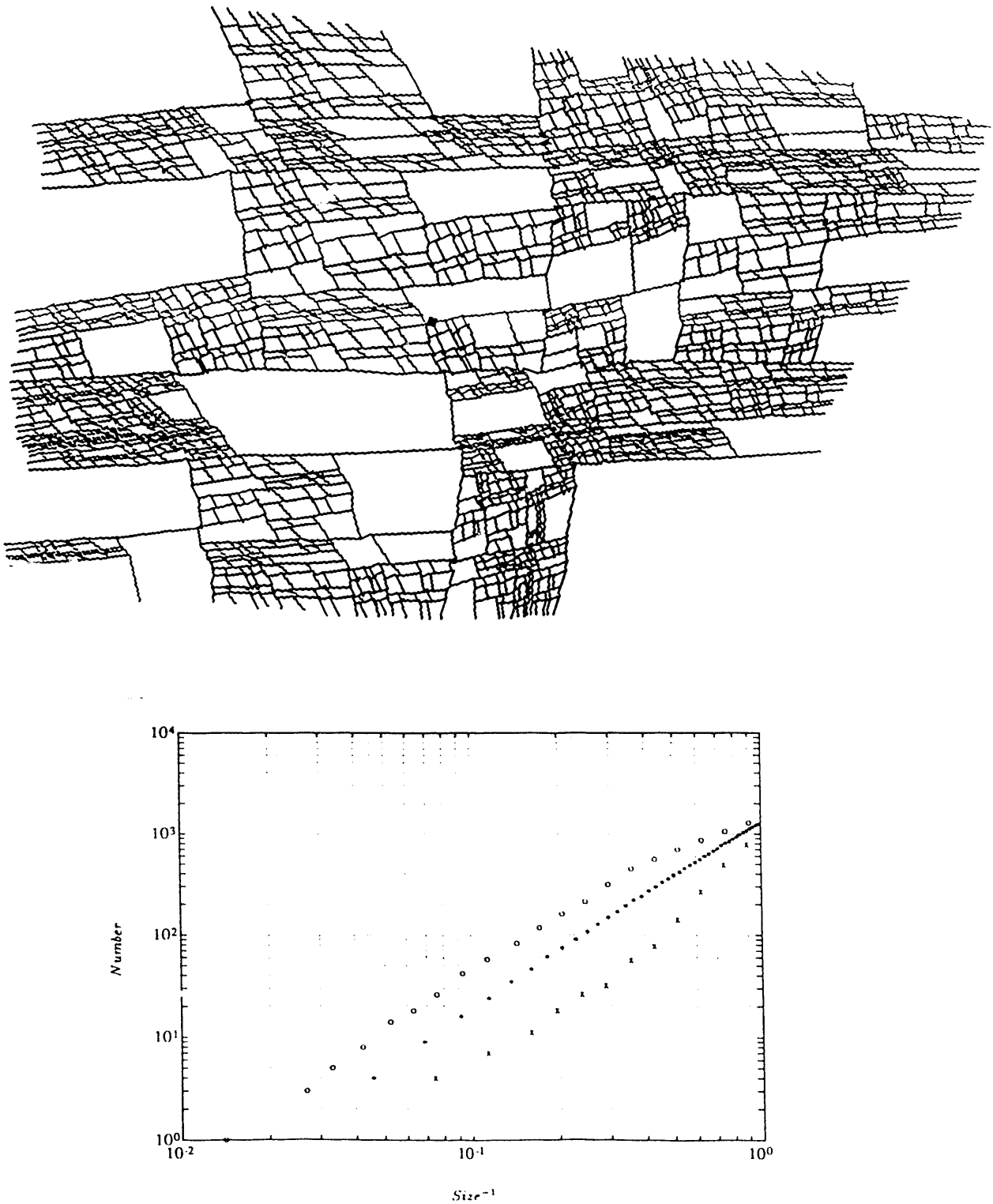

Figure 6: (a) Fracture network (11 generations) as in Figure 4 with $p_f = 0.90$. (b) Corresponding box counting($*$), fracture length(o) and fragment size (x) distributions.

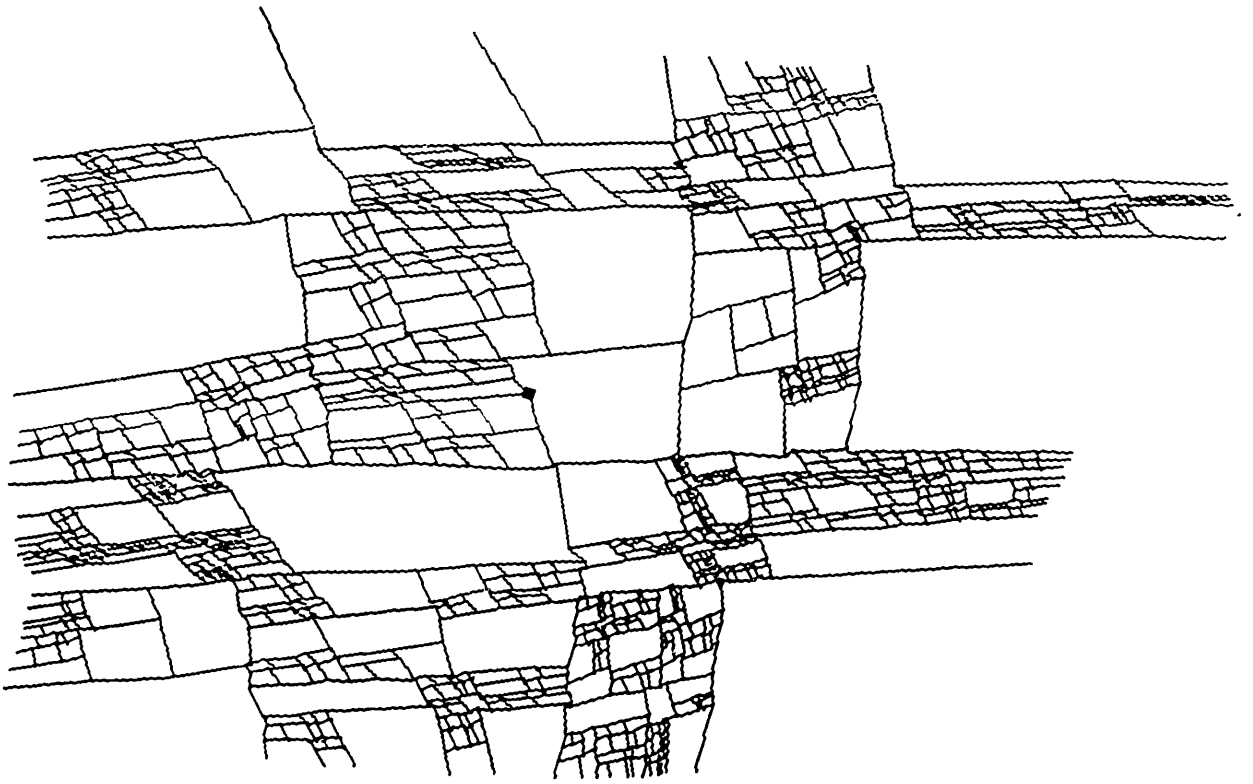

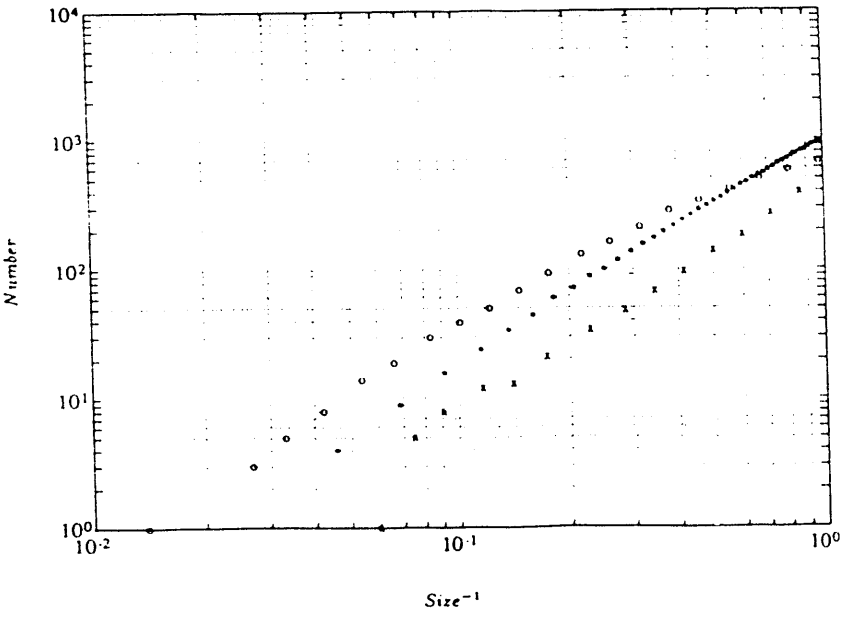

Figure 7: (a) Fracture network (11 generations) as in Figure 4 with $p_f = 0.80$. (b) Corresponding box counting($*$), fracture length(o) and fragment size (x) distributions.

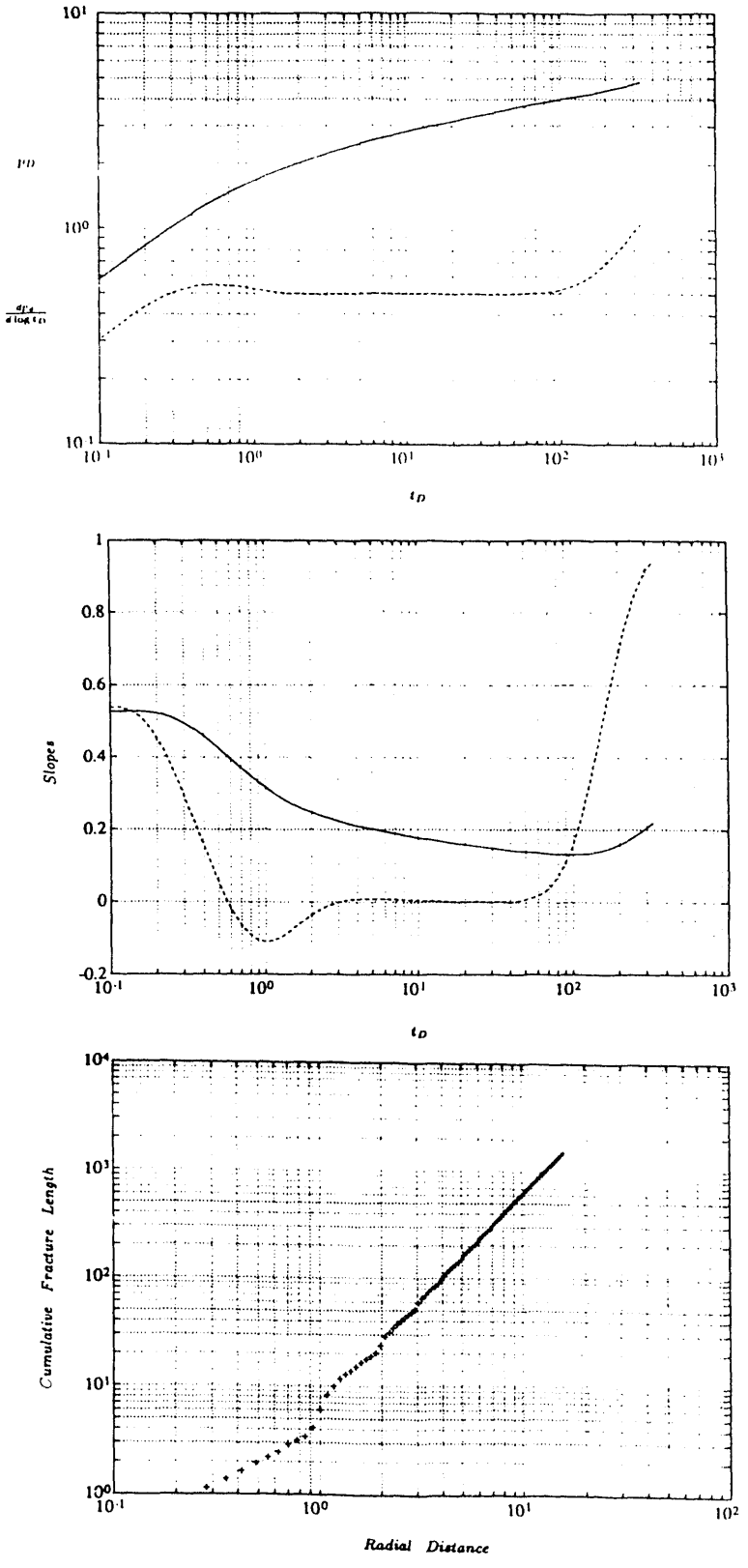

Figure 8: Pressure transient response for a homogeneous network. (a) Pressure (solid line), pressure derivative (dashed line). (b) Corresponding slopes. (c) Radial fracture mass plot.

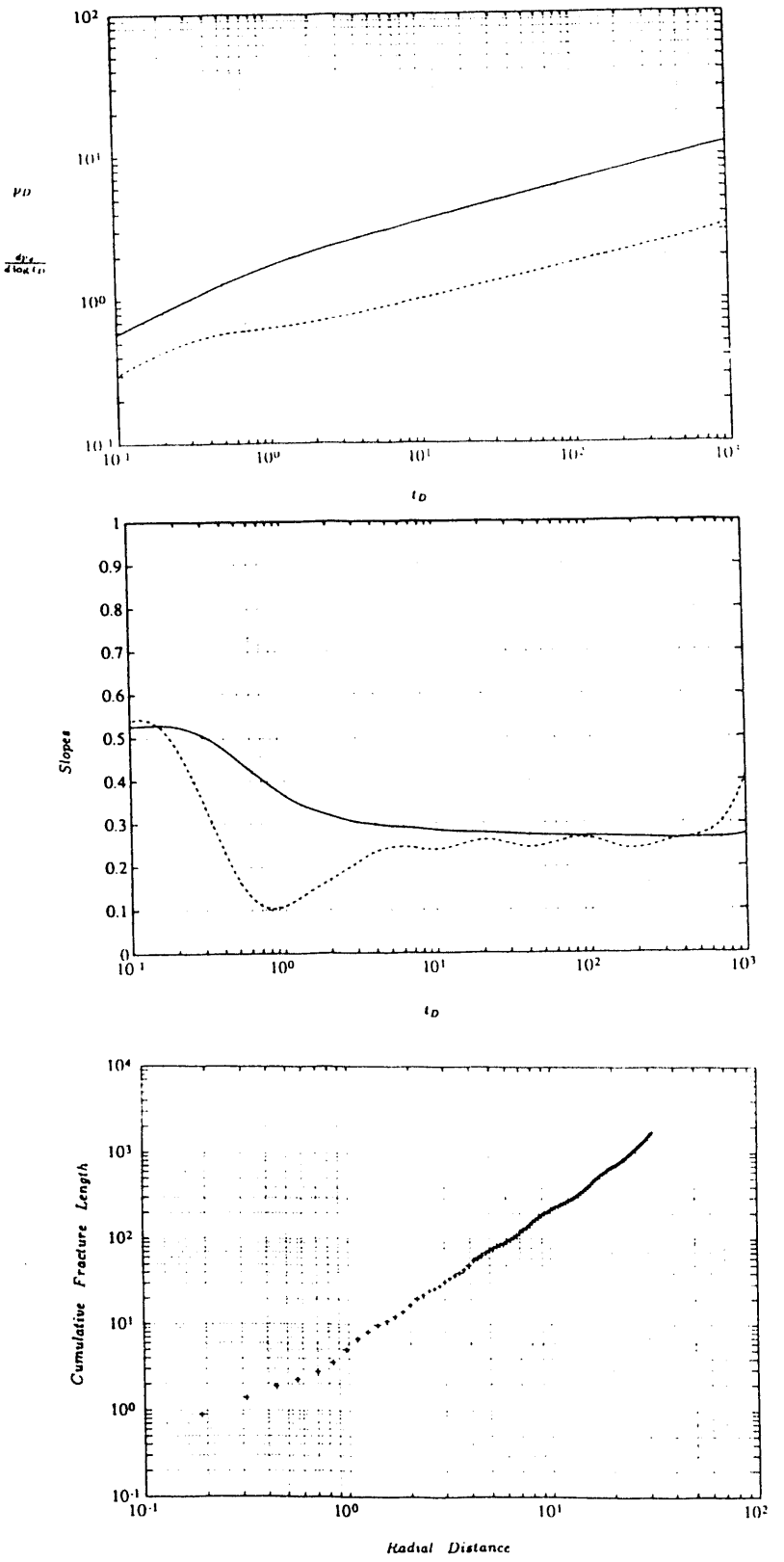

Figure 9: The response for the modified Sierpinski gasket of Figure 1a with well at A. (a), (b) Pressure transients. (c) Radial fracture mass plot for position A.

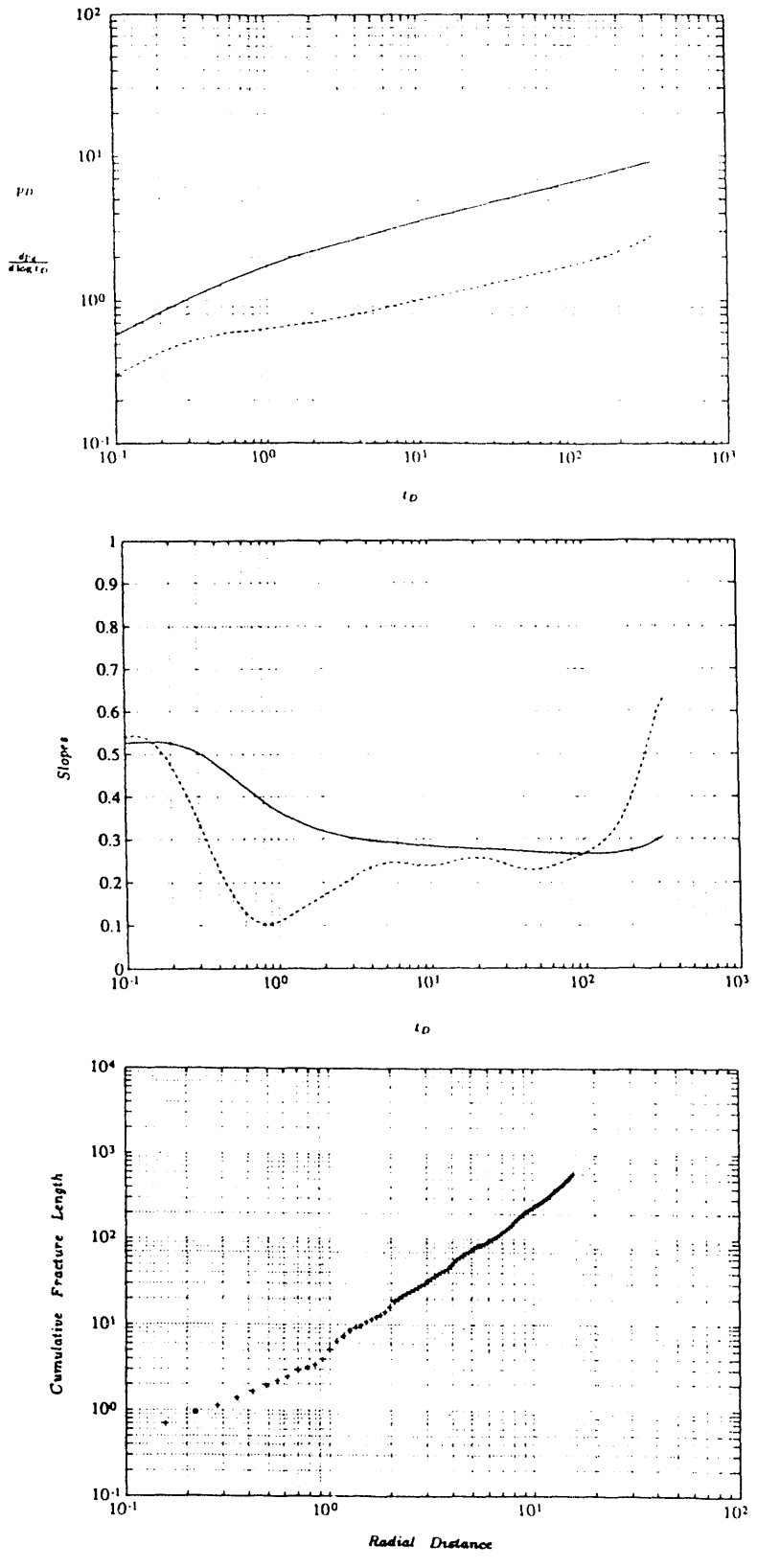

Figure 10: The response of the modified Sierpinski gasket (9 generations) with well at A. (a), (b) Pressure transients. (c) Radial fracture mass plot.

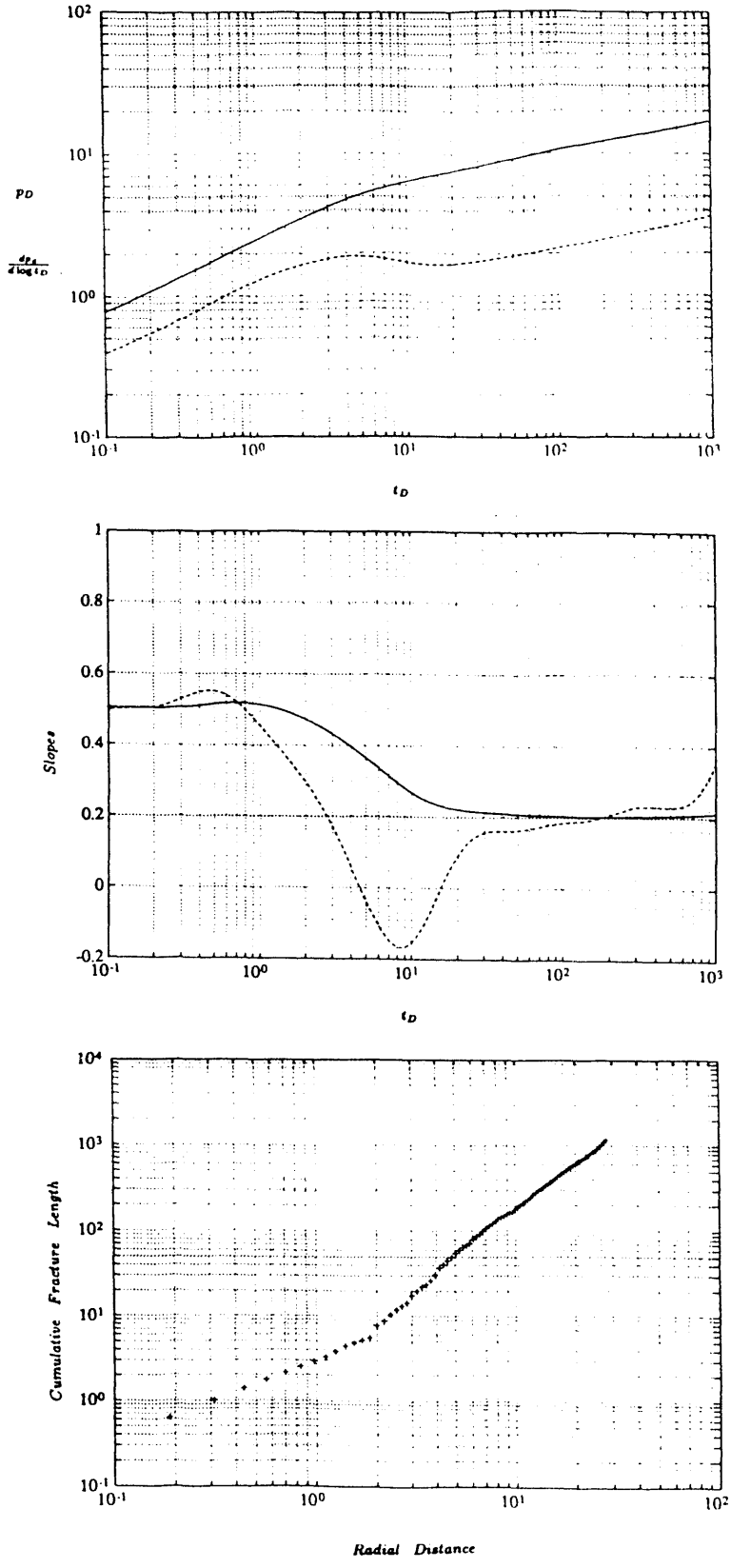

Figure 11: The response of the modified Sierpinski gasket of Figure 1a with well at B. (a), (b) Pressure transients. (c) Radial fracture mass plot for position B.

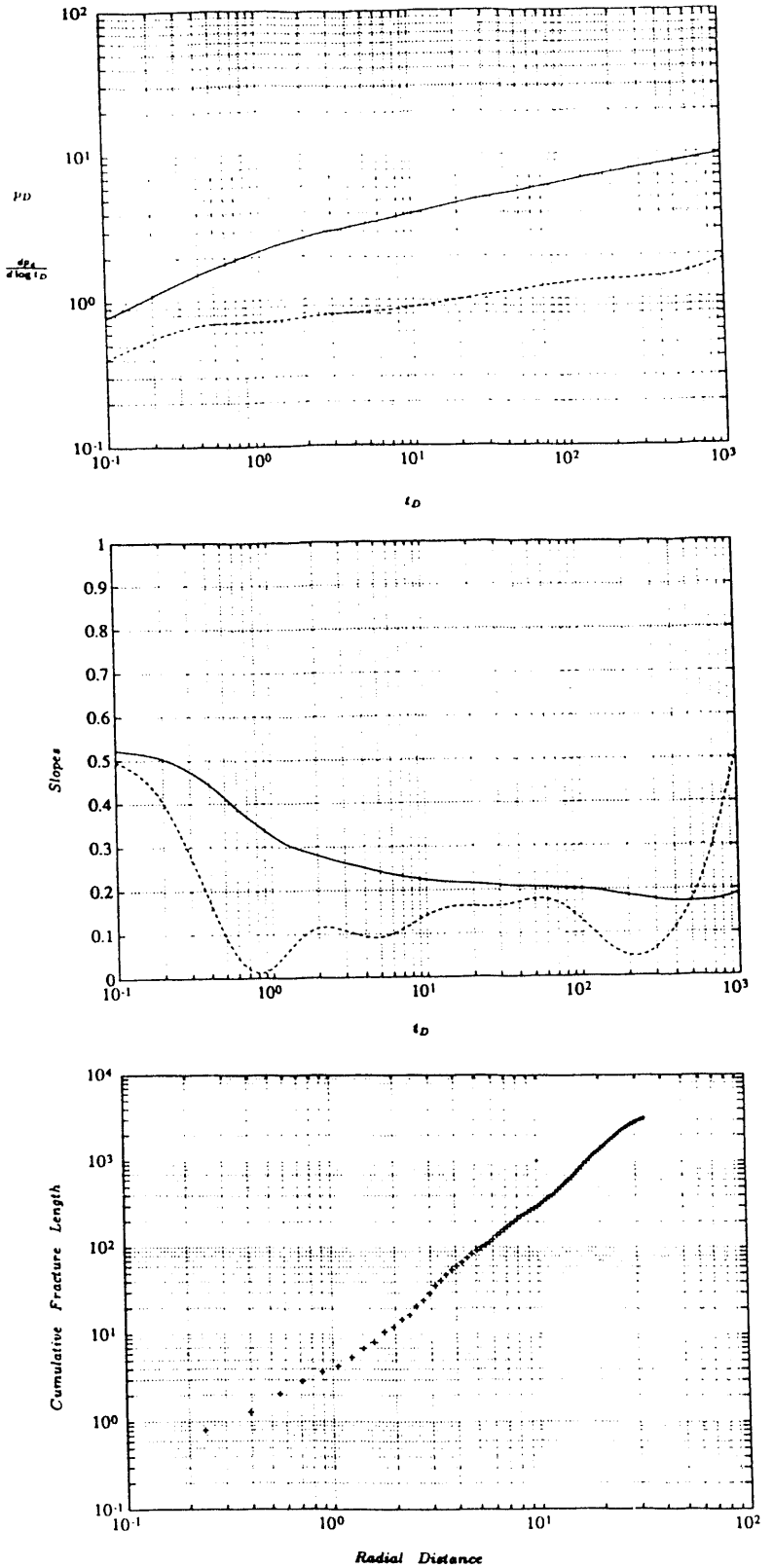

Figure 12: (a), (b) Pressure transient response for the network of Figure 6. (c) Radial fracture mass plot.

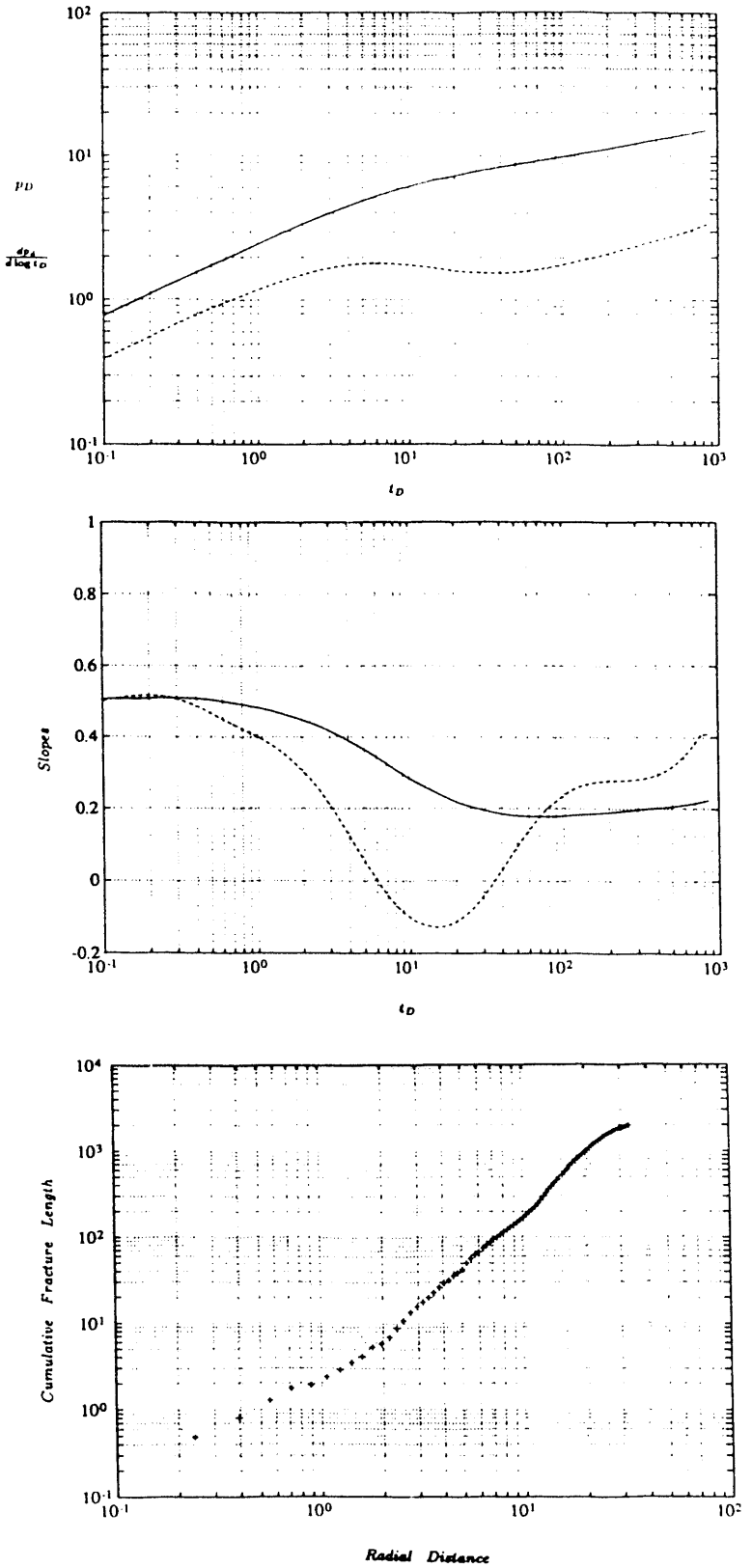

Figure 13: (a), (b) Pressure transient response for the network of Figure 7. (c) Radial fracture mass plot.

END

DATE FILMED

01/03/92